

# Electrochemical hydrogen storage properties of melt-spun $\text{Ti}_{0.9}\text{Zr}_{0.1}\text{V}_{0.2}\text{Ni}_{1.5}\text{La}_{0.5}$ alloy

Jian WANG<sup>1,2</sup>, Guang-bo CHE<sup>1</sup>, Qing-wei WANG<sup>1</sup>, Wan-xi ZHANG<sup>1</sup>, Li-min WANG<sup>1,2,†</sup>

<sup>1</sup>Key Laboratory of Preparation and Applications of Environmental Friendly Materials (Ministry of Education), Jilin Normal University, Siping 136000, China

<sup>2</sup>State Key Laboratory of Rare Earth Resource Utilization, Changchun Institute of Applied Chemistry, Chinese Academy of Sciences, Changchun 130022, China

E-mail: <sup>†</sup>lmwang@ciac.jl.cn

Received October 8, 2010; accepted January 24, 2011

The  $\text{Ti}_{0.9}\text{Zr}_{0.1}\text{V}_{0.2}\text{Ni}_{1.5}\text{La}_{0.5}$  alloy samples were synthesized by melt-spinning technique at the different wheel velocity (cooling rate), and the structure and electrochemical hydrogen storage properties were investigated. The result indicated that the structure of the melt-spun ribbons mainly contains C14 Laves phase and V-based solid solution phase. The discharge capacity, cyclic stability, high-rate discharge ability and electrochemical kinetic of the alloy electrodes are correlated with the cooling rate (wheel velocity), and the maximum discharge capacity is over 200 mA·h/g at the wheel velocity of 20 m/s.

**Keywords**  $\text{Ti}_{0.9}\text{Zr}_{0.1}\text{V}_{0.2}\text{Ni}_{1.5}\text{La}_{0.5}$  alloy, melt-spinning, hydrogen storage, electrochemical properties

**PACS numbers** 73.22.-f, 88.30.rd

## 1 Introduction

$\text{AB}_2$ -type alloys are regarded as a possible choice for hydrogen storage materials used for hydrogen suppliers, nickel–metal hydride batteries and the like in the future. In the past decades, increasing attention has been given to Ti–Ni  $\text{AB}_2$ -type hydrogen storage alloys consisting of multi-components as negative electrode materials for Ni–MH batteries because of their high energy density, high hydrogen storage capability, long life cycle and good environmental compatibility in comparison with metal hydrides [1–7].

Furthermore, the electrochemical properties of the Ti–Ni based alloys, a potential electrode, have been studied extensively [8, 9] and they are closely related to the phase structure, phase abundance and microstructures. It is well known that the two phases of the C14 Laves phase and the V-based solid solution phase, which have high hydrogen storage capacity and good hydrogen absorption and desorption kinetics at ambient environment due to the catalysis of the C14 phase to the V-based solid solution phase [10–12], have been applied in various hydrogen storage systems, except for the metal hydride electrode because of their poor electrochemical dis-

charge ability in alkaline electrolyte [13, 14]. Many methods have been carried out to improve the electrochemical properties, and among these methods the addition of various alloying elements and the melt-spinning have been proved to be the effective ways [15–18]. Named previously, the Zr, V and La elements are employed to partially substitute Ti and Ni in Ti–Ni  $\text{AB}_2$ -type alloy whereat the  $\text{Ti}_{0.9}\text{Zr}_{0.1}\text{V}_{0.2}\text{Ni}_{1.5}\text{La}_{0.5}$  is gained. The  $\text{Ti}_{0.9}\text{Zr}_{0.1}\text{V}_{0.2}\text{Ni}_{1.5}\text{La}_{0.5}$  alloy in block state is difficult to be crushed and the melt-spinning technique is a more useful method, compared with the other techniques, to prepare alloys with a composition that usually has higher hydrogen storage capacity, thereby easily crushed ribbons are obtained.

In this paper, one promising option is to change the cooling rates of quintuple alloy  $\text{Ti}_{0.9}\text{Zr}_{0.1}\text{V}_{0.2}\text{Ni}_{1.5}\text{La}_{0.5}$  by the melt-spinning technique. The impact of changing the cooling rates on the structure and the electrochemical hydrogen storage properties have been an object for investigation and the results will be discussed.

## 2 Experimental details

The  $\text{Ti}_{0.9}\text{Zr}_{0.1}\text{V}_{0.2}\text{Ni}_{1.5}\text{La}_{0.5}$  alloy was prepared through

arc-melting in water cooled copper furnace under a high purity argon atmosphere, and alloy ribbons were made by rapid solidification with a single roller melt-spinning technique at different wheel velocities in the range of 10–40 m/s. The crystalline phases of the melt-spun ribbons were determined by X-ray diffraction (XRD) with Cu  $K\alpha$  radiation. The working electrodes were constituted with 0.15 g alloy and 0.75 g carbonyl nickel powders made into a pellet of 10 mm in diameter and about 1.5 mm in thickness. The electrochemical properties were measured in a test cell composed of the alloy electrode using a sintered  $\text{Ni}(\text{OH})_2/\text{NiOOH}$  as counter electrode in 6 M KOH solution at 303 K. Charge and discharge test were carried out on automatic galvanostatic apparatus (DC-5). The electrodes were charged at a current density of 40 mA/g for 5.5 h and then discharged at a current density of 13.3 mA/g. The electrochemical impedance spectroscopy (EIS) analysis was conducted at the 50% depth of discharge (DOD).

### 3 Results and discussion

#### 3.1 Structure characteristics

Figure 1 shows the XRD patterns of as-cast and melt-spun alloy samples with different wheel velocities. It exhibited that the melt-spun ribbons caused a significant change of phase structure, which confirms that narrower and sharper diffraction peaks are found in the melt-spun ribbons as compared with the as-cast sample, and the intensity and quantity of diffraction peaks correspond to the increasing cooling rate (wheel velocity). It can be seen that the melt-spun alloy ribbons exhibited similar diffraction patterns, which can be assigned to BCC, C14 Laves, Ti–Ni and  $\text{LaNi}_5$  phases. This indicates that the phase constitution remains almost unchanged at different cooling rate, except that multi-component alloys are both amorphous and crystalline structures coexistent in

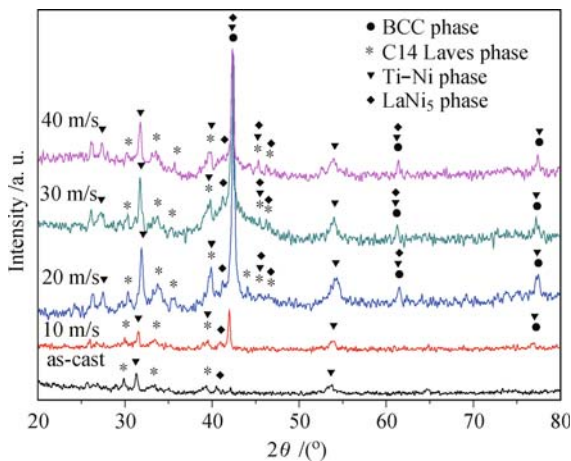


**Fig. 1** XRD of  $\text{Ti}_{0.9}\text{Zr}_{0.1}\text{V}_{0.2}\text{Ni}_{1.5}\text{La}_{0.5}$  alloy with different wheel velocities.

the melt-spun alloy ribbons fabricated with the wheel velocity of 30 m/s and 40 m/s. In addition, the two phases of BCC type of V-based solid solution phase and C14 Laves phase in the melt-spun alloy samples can be clearly identified, especially at the wheel velocity of 10 m/s and 20 m/s.

#### 3.2 Activation and maximum capacity

Figure 2 displays the dependence of discharge capacity on cycle number for as-cast and melt-spun  $\text{Ti}_{0.9}\text{Zr}_{0.1}\text{V}_{0.2}\text{Ni}_{1.5}\text{La}_{0.5}$  alloy electrodes. The electrochemical properties of the electrodes are shown in Table 1. The activation capability, which is very important for the practical use of Ni–MH battery, was characterized by the number of charge–discharge required for attaining the greatest discharge capacity through a charge–discharge cycle at a constant current density. The fewer the cycle number, the better the activation performance. The influences of spinning rate on the activation capabilities of the alloy electrodes are shown in Fig. 2, respectively.

**Table 1** Electrochemical performance of  $\text{Ti}_{0.9}\text{Zr}_{0.1}\text{V}_{0.2}\text{Ni}_{1.5}\text{La}_{0.5}$  alloy electrodes with different rates.

Sample	$C_{\text{max}}/(\text{mA}\cdot\text{h}/\text{g})$	CR/(%) <sub>24h</sub>	HRD <sub>160</sub> <sup>a</sup> /%	$N_a^b$	$S_{40}/\%$
as-cast	62.95	91.26	22.80	6	22.08
10 m/s	133.0	90.88	50.25	11	74.61
20 m/s	203.4	89.78	57.34	7	75.36
30 m/s	189.6	92.47	67.35	4	95.25
40 m/s	173.3	91.65	66.41	3	90.10

<sup>a</sup> The high-rate dischargeability at the discharge current density of 160 mA/g.

<sup>b</sup> The number of cycles needed to activate the electrode.

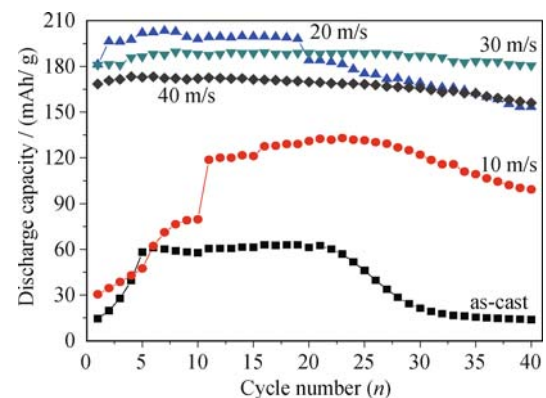


**Fig. 2** Discharge capacities as a function of cycle number for  $\text{Ti}_{0.9}\text{Zr}_{0.1}\text{V}_{0.2}\text{Ni}_{1.5}\text{La}_{0.5}$  alloy electrodes with different wheel velocities.

It exhibited that the activation property is dramatically enhanced by melt-spun alloy ribbons and the activation cycle number decreases with the increase of the wheel velocity (cooling rate). Compared with the as-cast alloy sample, the melt-spun alloy ribbons have a higher electrochemical charge/discharge capacity, especially at

the wheel velocity of 20 m/s, where the melt-spun specimen shows an excellent electrochemical capacity of 203 mA·h/g. Moreover, in this work we have found that the great span with capacity got improved when the cooling rate increases from as-cast state to the wheel velocity of 20 m/s, and decreases afterwards when the wheel velocity reaches 40 m/s. This might be related to the phase composition of the obtained alloy. Further investigation to elucidate this is in progress.

It is noteworthy that melt-spinning engenders a stronger impact on the maximum discharge capacity of the melt-spun alloy samples than that of the as-cast alloy samples. Some explanations are herein offered as the reason why melt-spinning significantly enhance the discharge capacity for the alloy. The increased discharge capacity is attributed to the enhanced crystalline phase forming ability of the alloy through melt-spinning. All kinds of the crystalline phases, which are the Ti-Ni phase, LaNi<sub>5</sub> phase, and particularly the two phases of V-based BCC solid solution phase and C14 Laves phase, provided a transcendent discharge property to the alloy. On all accounts, a proper cooling rate sealed a preminent discharge property for the melt-spun alloy ribbons.

### 3.3 Cyclic stability

The cyclic stability of the Ti<sub>0.9</sub>Zr<sub>0.1</sub>V<sub>0.2</sub>Ni<sub>1.5</sub>La<sub>0.5</sub> alloy electrodes are also shown in Fig. 2. It indicated that the capacity retentions of the melt-spun alloy ribbons at different wheel velocities are excellent in comparison to the as-cast samples. The capacity retention used to represent the life cycle performance can be calculated with the following equation:

$$S_n(\%) = 100 \times \frac{C_n}{C_{\max}} \quad (1)$$

where  $S_n$  is the capacity retention at  $n$  cycles,  $C_n$  the discharge capacity at  $n$  cycles and  $C_{\max}$  the maximum discharge capacity. It is proved that the capacity retention of the Ti<sub>0.9</sub>Zr<sub>0.1</sub>V<sub>0.2</sub>Ni<sub>1.5</sub>La<sub>0.5</sub> alloy electrodes after 40 circles increases first with the increase of the cooling rate, and then decreases when the cooling rate of the melt-spun alloy samples further increases. However, it seems that it did not present clear enough, orderly self-discharge properties. After the original test of 40 successive cycles of charging/discharging, the cycling

**Table 2** Electrochemical kinetic parameters of melt-spun Ti<sub>0.9</sub>Zr<sub>0.1</sub>V<sub>0.2</sub>Ni<sub>1.5</sub>La<sub>0.5</sub> alloy electrodes with different wheel velocities.

Sample	Charge-transfer Resistance $R_{ct}/\Omega$	Exchange current density $I/\text{mA}$
10 m/s	4.373	5.970
20 m/s	1.835	14.28
30 m/s	1.926	13.56
40 m/s	2.611	10.00

capacity retention rates for the melt-spun alloy electrodes were above 74%, and the cooling rate of 40 m/s shows the best life cycle.

The laggard degradation of cycle stability could be explained by the existence of the Ti, Zr and La elements with Ni forms LaNi<sub>5</sub>, whose life cycle would be lengthened in KOH electrolyte. The charge retention values were summed up in Table 1.

### 3.4 High-rate dischargeability and electrochemical kinetics

Figure 3 illustrates the relationship between the HRD and the discharge current of as-cast and melt-spun alloy electrodes at 303 K.

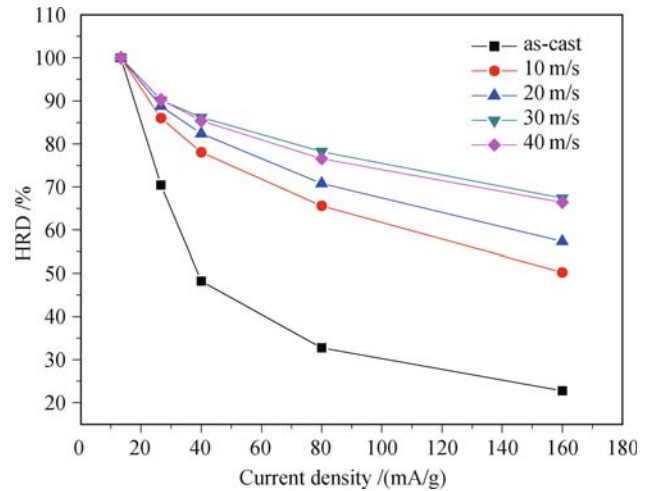


**Fig. 3** High-rate dischargeability of as-cast and melt-spun Ti<sub>0.9</sub>Zr<sub>0.1</sub>V<sub>0.2</sub>Ni<sub>1.5</sub>La<sub>0.5</sub> alloy electrodes with different rates.

The values of HRD were calculated from the following equation [19]:

$$\text{HRD} = \frac{C_d}{C_{13.3}} \times 100\% \quad (2)$$

where  $C_d$  is the discharge capacity at the discharge current density  $I_d$ ,  $C_{13.3}$  is the discharge capacity at a discharge current of 13.3 mA/g also after the alloy electrode has been fully discharged at the discharge current density ( $I_d$ ). From Fig. 3, we can see clearly that when the electrode is discharged at current densities ( $I_d$ ) as 13.3–160 mA/g, the HRD of the alloy electrodes increase with the increasing cooling rates, which was not obviously affected by the wheel velocities of 30 m/s and 40 m/s.

It is well known that the HRD of the metal hydride electrodes are influenced mainly by the charge-transfer reaction occurring at the electrode/electrolyte interface [20]. In general, the charge-transfer reaction was dominated by charge-transfer resistance at the electrode/electrolyte interface or the exchange current density.

In order to further reveal the relationship between the

electrochemical kinetics and the melt-spun alloy samples, the EIS of the alloy electrodes with different spun cooling rates at 50% DOD and 303 K were performed and shown in Fig. 4. It can be seen that the EIS consists of two semicircles and a straight line upon the samples. According to the model proposed by Kuriyama *et al.* [20], the smaller semicircle in the higher frequency region is mainly related to the resistance and capacitance between the alloy particles and the current collector, while the larger semicircle in the lower frequency region is attributed to the charge-transfer resistance for hydrogenation reaction at the interface.

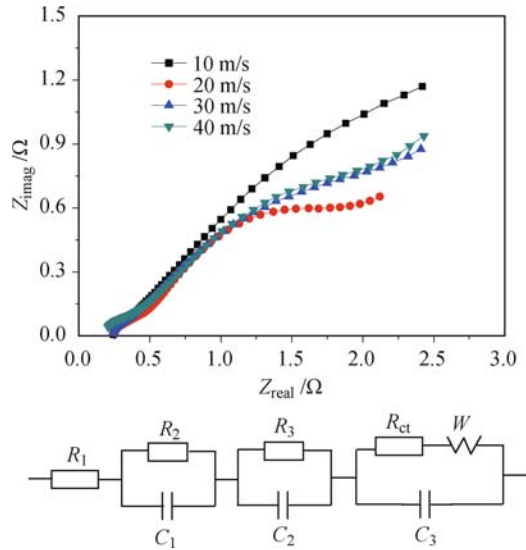


**Fig. 4** Electrochemical impedance spectra of  $\text{Ti}_{0.9}\text{Zr}_{0.1}\text{V}_{0.2}\text{Ni}_{1.5}\text{La}_{0.5}$  alloy electrodes with different wheel velocities.

In Fig. 4, except for the wheel velocity of 10 m/s, the radius of the larger semicircle in the low frequency region decreased with the decrease of the cooling rate, which means a decline in the charge-transfer resistance of interface along with the decreasing cooling rate. The minimum charge-transfer resistance was obtained at the wheel velocity of 20 m/s. These results are in good agreement with the above mentioned behavior of HRD. Simultaneously, the exchange current density curves of the  $\text{Ti}_{0.9}\text{Zr}_{0.1}\text{V}_{0.2}\text{Ni}_{1.5}\text{La}_{0.5}$  alloy electrodes with different cooling rates were also achieved at 50% DOD and 303 K, which can be calculated by the following formula and are shown in Fig. 4:

$$I_0 = \frac{RT}{FR_{ct}} \quad (3)$$

where  $R$ ,  $T$  and  $F$  denote the gas constant, the absolute temperature and the Faraday constant, respectively. It can be seen from Table 2 that the exchange current density of the melt-spun alloy samples increases first and then decreases as the cooling rate increases. The exchange current density results agree with the HRD behavior of the electrode.

## 4 Conclusions

The electrochemical properties of  $\text{Ti}_{0.9}\text{Zr}_{0.1}\text{V}_{0.2}\text{Ni}_{1.5}\text{La}_{0.5}$  hydrogen storage alloys electrodes are affected markedly by the melt-spinning technique. All the melt-spun alloy samples are mainly composed of the C14 Laves phase, the BCC V-based solid solution phase, Ti-Ni and  $\text{LaNi}_5$  phases. With the increase of the cooling rate (wheel velocity) from 10 m/s to 40 m/s, the maximum discharge capacity increased from 62.95 mA·h/g to 203.4 mA·h/g (20 m/s) and then decreases to 173.3 mA·h/g (40 m/s). And the charge retention rate and the cycling stability investigations further confirm the change tendency of the electrochemical properties for the alloy electrodes with different cooling rates.

The HRD of the alloy electrodes increases with the increase of the cooling rate. Moreover, the EIS of the melt-spun alloy electrodes increased in the charge-transfer resistance of interface with the increasing cooling rate. The minimum charge-transfer resistance was obtained at the wheel velocity of 20 m/s. It can be attributed to the abundant existence of C14 Laves phase, which has an ameliorated electrocatalytic activity for the charge transfer reaction of metal hydride electrode.

**Acknowledgements** This work was supported by the Key Laboratory of Preparation and Applications of Environmental Friendly Materials (Ministry of Education) and the Foundation for Innovative Research Groups of the National Natural Science Foundation of China (Grant No. 20921002).

## References

1. H. W. Yang, W. S. Lee, Y. Y. Wang, C. C. Wan, T. W. Cheng, and K. H. Lang, *J. Mater. Res.*, 1995, 10(7): 1680
2. D. Y. Song, X. Q. Gao, Y. S. Zhang, J. Yan, and P. W. Shen, *J. Alloys Comp.*, 1994, 206(1): 43
3. Z. B. Liu, Q. Li, Z. Zhang, G. F. Mi, Q. L. Yuan, and L. M. Wang, *Int. J. Hydrogen Energy*, 2009, 34(4): 1890
4. D. Y. Yah, G. Sandrock, and S. Suda, *J. Alloys Comp.*, 1995, 223(1): 32
5. S. M. Lee, S. H. Kim, and J. Y. Lee, *J. Alloys Comp.*, 2002, 330-332: 796
6. H. H. Lee, K. Y. Lee, and J. Y. Lee, *J. Alloys Comp.*, 1997, 253-254(1-2): 601
7. S. J. Choi, J. Choi, C. Y. Seo, and C. N. Park, *J. Alloys Comp.*, 2003, 356-357: 725
8. B. Z. Liu, Y. M. Wu, and L. M. Wang, *J. Power Sources*, 2006, 159(2): 1458
9. W. Hu, J. L. Wang, L. D. Wang, Y. M. Wu, and L. Wang, *Electrochim. Acta*, 2009, 54(10): 2770
10. H. Iba and E. Akiba, *J. Alloys Comp.*, 1997, 253-254(1-2): 21
11. M. Tsukahara, K. Takahashi, T. Mishima, A. Isomura, and T. Sakai, *J. Alloys Comp.*, 1997, 253-254(1-2): 583

12. M. Tsukahara, K. Takahashi, T. Mishima, A. Isomura, and T. Sakai, *J. Alloys Comp.*, 1996, 236(1–2): 151
13. Y. H. Xua, C. P. Chen, X. L. Wang, Y. Q. Lei, X. H. Wang, L. X. Chen, and Q. D. Wang, *Int. J. Hydrogen Energy*, 2007, 32(12): 1716
14. J. J. Reilly and R. H. Wiswall, *Inorg. Chem.*, 1979, 9(7): 1678
15. Q. A. Zhang, Y. Q. Lei, X. G. Yang, Y. L. Du, and Q. D. Wang, *Int. J. Hydrogen Energy*, 2000, 25(10): 977
16. H. Miao, M. X. Gao, Y. F. Liu, Y. Lin, J. H. Wang, and H. G. Pan, *Int. J. Hydrogen Energy*, 2007, 32(16): 3947
17. Y. H. Zhang, B. W. Li, H. P. Ren, S. H. Guo, Z. W. Wu, and X. L. Wang, *Mater. Chem. Phys.*, 2009, 115(1): 328
18. T. Z. Huang, Z. Wu, S. L. Feng, B. J. Xia, and N. X. Xu, *Mater. Sci. Eng. A*, 2005, 390(1–2): 362
19. K. Zhong, Y. F. Liu, M. X. Gao, J. H. Wang, H. Miao, and H. G. Pan, *Int. J. Hydrogen Energy*, 2008, 33(2): 149
20. N. Kuriyama, T. Sakai, H. Miyamura, I. Ueharaand, and H. Ishikawa, *J. Alloys Comp.*, 1993, 202(1–2): 183